Eko Sasmito Hadi
Tuswan Tuswan
Ghina Azizah
Baharuddin Ali
Samuel Samuel
Muhammad Luqman Hakim
Muhammad Raaflie Caesar Putra Hadi
Muhammad Iqbal
Dian Purnama Sari
Dendy Satrio

http://dx.doi.org/10.21278/brod74107

ISSN 0007-215X
eISSN 1845-5859

Influence of the canal width and depth on the resistance of 750 DWT Perintis ship using CFD simulation

UDC 629.5.015.2:(282.5)
Original scientific paper

Summary

Investigation of hydrodynamic interaction between the vessel and the seabed when entering shallow water is considered one of the most critical considerations of inland waterway transport. There are many investigations into the behavior of ships in restricted waters, such as ships traveling in different forms of canal cross-sections. The present study aims to evaluate the hydrodynamic interaction of the 750 DWT Perintis Ship moving through the different canal types to determine the relative effects of limiting the width and depth cross section on the ship's resistance. Two different canals with different cross sections, including canal bank and rectangular canal, were evaluated to investigate the influence of canal width (W_b), depth ratio (h_w/T), and blockage ratio function (A_s/A_c). The Computational Fluid Dynamic (CFD) method with Reynolds-averaged Navier–Stokes (RANS) solver and turbulent model $k-\varepsilon$ were used to predict the total resistance of the ship. The proposed numerical simulation was initially validated with an experimental towing tank test in the error range of 0.11-7.74%. The results indicated similar phenomena were found both in rectangular and canal banks. The case with a shallower (lower h_w/T) and a narrower (lower B_c/B_s) canal dimension has a higher resistance value. Backflow and subsidence of free surface became significant around the ship's hull in more restricted water, changing the ship's hydrodynamic characteristics and increasing resistance. It can be found that the higher the blockage ratio (m_b), the higher the total resistance value in both canal types, which proved that ships with higher speeds were more sensitive to changes in waterway restrictions.

Keywords: Canal; Restricted Waters; 750 DWT Perintis; Ship Resistance

1. Introduction

Several remote islands in Indonesia have long lacked the infrastructure required for resource distribution. As a result, basic supplies are scarce on these islands, and prices are higher than on the main islands. Under Presidential Decree Number 106 of 2015 & Decree from the Ministry of Transportation Number 4 of 2016, the Indonesian government established a sea toll initiative to accelerate domestic demand growth and speed up inter-island travel by developing sea infrastructure [1]. Most ships used to increase infrastructure and connectivity are purpose-built under the order of the government. The 750 DWT Perintis Ship is part of the initiative, a type of passenger ship controlled by the state as part of the sea toll project to promote inland connectivity with restricted waterways in Eastern Indonesia [2, 3]. Given that shipping routes regularly pass through shallow water, it's worth investigating how the hydrodynamics characteristics of the 750 DWT Perintis model affect ship resistance.

Ship behaviour changes due to hydrodynamic interactions between the ship's hull and the bottom of the water when operating in restricted waters [4, 5]. The effect of water depth on the derivative of ship stability can be explained by increasing the additional mass of the lateral cross-section in shallow water. This effect is even more substantial in the canal [6]. According to the experience of ship operators, a ship sailing in restricted waters loses speed, increases fuel consumption, and risks colliding with the canal's bottom. The ship loses around 30% of its speed when travelling in shallow water and up to 60% in restricted waters [7]. In restricted waters, the flow around the hull changes compared to open waters due to bottom and fairway edge effects, which results in increased backflow, a more substantial squat effect, and changes in the wave pattern generated by the vessel [8]. However, most merchant ships have low speed and poor flexibility. The possibility of collision is high in restricted water [9].

Previous research landmarks on numerically investigating ship behaviour on restricted water were reviewed in detail. Several studies typically focus on resistance, ship-generated waves, squats, and maneuverability to explore the effect of restricted environments. Firstly, using the CFD-based method, Campbell et al. [10] analyzed the impact of increasing trim and draft on the ship's drag when travelling through restricted waterways. The results showed that increasing the draft increases the hydrodynamic resistance by about 10-15%, depending on the ship's speed range. Due to the change in the flow field, the accelerated fluid causes an increase in the hydrodynamic force on the vessel [11]. Moustafa and Yehia [12] studied the effect of squat in shallow water on River Nile cruisers in Luxor-Aswan. The findings reveal the position and amplitude of the maximal squat, as well as the grounding speed. It has been discovered that masters' understanding of the squat phenomena and its prediction for each unique vessel is of major significance for vessel safety [13]. Moreover, Ahmed et al. [14] conducted a CFD-based analysis to evaluate the shallow water impacts on prismatic planing hulls by comparing the hydrodynamics of a prismatic planing flat bottom hull operating in a shallow water channel to its hydrodynamics in open water. Consequently, the worst effect on the planing hull in a shallow channel comes at critical speeds where a solitary wave forms. As a result, boat drivers must avoid sailing at crucial speeds. In addition, several previous investigations on ship-generated waves [15] and maneuverability characteristics [16] in shallow water and narrow channel can be reviewed.

The ship's resistance in shallow water is found to be higher than the ship sailing in deep water [17-20]. Hoa et al. [21] presented work to investigate the effect of water depth on ship resistance US of Navy Combatant DTMB using the CFD method. The study showed that the resistance value in shallow water was higher at the same speed than in deep water. This phenomenon was caused by changes in flow velocity in the bottom area and a significant decrease in pressure around the hull. Chen et al. [22], in their experiments on the effect of water

depth and the speed range from medium to very shallow waters, showed that limiting water depth changes the pressure distribution around the ship significantly, increasing the drag force and reducing maneuverability. Moreover, Park et al. [23] used the numerical method to determine hydrodynamic forces' effect on passing and moored ships in shallow waters. The study showed that when the water depth decreases, the hydrodynamic load of the ship increases, especially in shallow water conditions where the depth ratio (h_w/T) is < 1.2.

The resistance value increases as the canal width dimension decreases [24]. The forces and moments in the ship's hull due to pressure variations when the ship travels close to the shore are called the bank effect. A reduced canal cross-section can result in a pressure drop [25]. The experimental results of Elsherbiny et al. [26] regarding the analysis of squat, trim, and resistance on the geometry of the Suez canal (canal bank) and rectangular canal geometry showed that with a reduction in width, there was an increase in the total resistance coefficient. It can be explained that when the ship enters the canal, there is an increase in the flow velocity in the canal, which increases the value of the total resistance coefficient.

An extended study on CFD-based simulation was conducted to analyze the influence of the canal bank geometry with various water depth conditions, draft, and ship speed on obstacles and ship-generated waves in confined water/space [11]. This study shows that the highest ship's resistance has occurred when operating in shallow, narrow water conditions and when the ship's draft is highest. In addition, complex wave patterns in closed canal lines are captured in the simulation, where wave reflections and interference can be observed. Tezdogan et al. [27] showed the results of numerical simulations predicting the squat and drag of the model-scale ship moving forward on the asymmetric canal. Moreover, by varying the ship's draft at various speeds, Elsherbiny et al. [28] studied the performance of container ships travelling on a rectangular cross-sectional geometry of the Suez Canal, which was analyzed in different methods, experimentally, CFD, the slender body theory, and empirical formulas. The results revealed a strong coupling between the canal cross-section and all evaluated parameters. In addition, Terziev et al. [29] studied the effect of currents on ship performance in confined waters. They recommended saving fuel, one of which is by varying the water depth and the width of the canal to estimate the effect of the geometric properties of the waterways.

Based on previous work, the CFD method yields good results when solving the problem of the ship's hydrodynamic characteristics in restricted water conditions. This method allows the visualization of quantities that are difficult to obtain experimentally, such as streamlined flow, wave profiles, and pressure distributions. In the ship resistance issue, the average value of the force should be emphasized. Using the term "turbulence model," the RANS method simulates turbulence and provides time-averaged values for velocity and pressure [30]. Therefore, it requires less time and fewer computational resources [31].

Based on the above-mentioned studies, the differences in the ship hull form and operating conditions cause unique ship hydrodynamic phenomena. Therefore, an extended investigation of the effect of the different cross-sections of the various canal types on the resistance increase and wave characteristic is critical to investigate using the newly developed Perintis hull form model. This current work aims to analyze the effect of canal width, depth, and velocity variations using the CFD method with the variations of canal types. The geometry of selected canal types will be investigated, including canal banks and rectangular canal cross-sections assumed to be restricted waters or rivers. Benchmark study is initially conducted by comparing developed CFD simulation with towing tank experiment at different speed ranges. The result of ship hydrodynamic characteristics was reviewed in detail to measure the effect of canal width (W_b), depth ratio (h_w/T), and blockage ratio function (A_s/A_c) on the resistance and wave-generated characteristics of the 750 DWT Perintis Ship model.

2. Ship Geometry and Numerical Simulation

2.1 Ship Model Geometry

This current study used the 750 DWT Perintis Ship as a reference model [1]. The full-scale model was scaled with a scale factor of 1:18 using Rhinoceros and DELFTship software to perform the simulation. The model verification of the 3D hull shape was determined by comparing the principal dimension and hydrostatic values such as displacement, *Cb*, *LCB*, etc. Fig. 1 and 2 depict the ship's hull geometry and lines plan, and the main dimension is presented in Table 1. To validate the resistance results from the CFD method, the 750 DWT Perintis model was experimentally tested by the Indonesian Hydrodynamic Laboratory (IHL) by conducting a resistance test based on the International Towing Tank Conference (ITTC) standard.

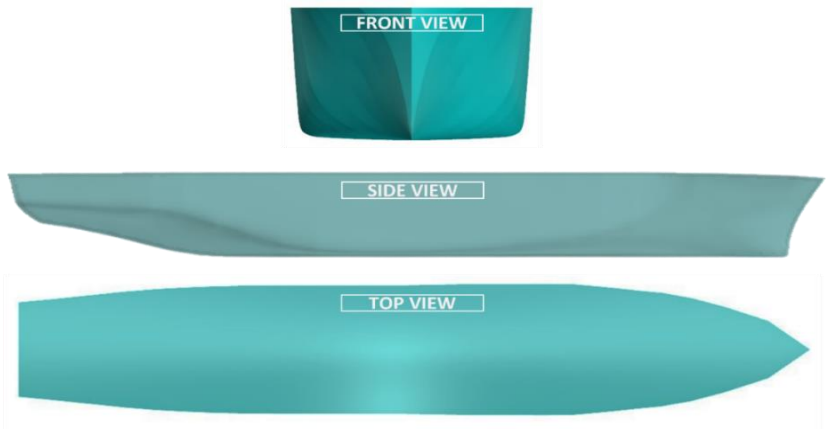

Fig. 1 Three-dimensional model of 750 DWT Perintis Ship.

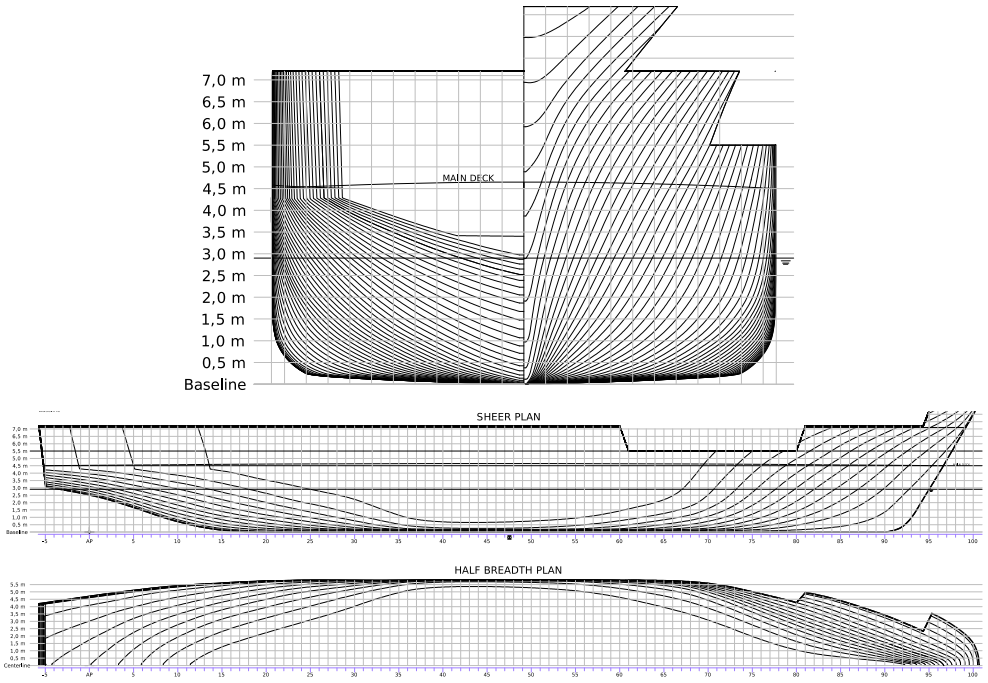

Fig. 2 750 DWT Perintis Ship lines plan.

Table 1. Comparison of main ship dimension between full-scale and model-scale

Ship main dimensions	Full-scale	Model (1:18)	Unit
Length of water line, *Lwl*	57.0	3.27	m
Breadth, *B*	11.6	0.64	m
Draft, *T*	2.9	0.16	m
Height, *H*	4.5	0.25	m
Displacement, Δ	1163	0.20	ton
Midship coefficient, (C_m)	0.94	0.94	-
Block coefficient (C_B)	0.57	0.57	-

2.2 Parameter of Numerical Simulations

The ship resistance analysis was simulated in different computational domains: canal banks and rectangular geometry [28]. The numerical setup was initially validated by comparing the computational results to the IHL towing tank experimental model test data using the total resistance value to validate the computational results. In this investigation, the two canal geometries represent restricted waters or rivers. In each canal geometry, simulations were conducted with two water depths (h_w/T), two canal widths (W_b), and five velocity variations under calm water and even keel conditions.

The parameters generated eight simulation cases for two different canal types are displayed in Tables 3 and 4. Table 3 presents the parameter of four simulation cases (Cases I-IV) for the canal bank type, and Table 4 presents the parameter of four cases (Cases V-VIII) for the rectangular canal type. This study examined the effects of varying canal depth (h_w/T) and width (W_b) on the ship's resistance while moving through different canal types. There were two canal depth parameters, h_w/T = 2.24 representing shallow water and canal depth parameters h_w/T = 16.15 representing deep water conditions [28]. The canal width parameters W_b = 2.4 m and W_b = 4.8 m were applied to the bottom of the canal. Table 2 displays the speed range (*Vs*) and *Fr* used in this investigation, which ranges from 12 to 17 knots at the full-scale model. To demonstrate the relationship between ship resistance and speed, the Froude Number (*Fr*) and depth Froude Number (F_{rh}) were utilized, transforming the speed factor into a non-dimensional quantity. The Froude Number and depth Froude Number were calculated using Eq. 1 & 2 [20]:

$$F_r = \frac{U_\infty}{\sqrt{gL}} \tag{1}$$

$$F_{rh} = \frac{U_\infty}{\sqrt{gh}} \tag{2}$$

where U_∞ is the speed of the ship (m/s), g is the acceleration due to gravity 9.81 m/s^2, L is the length of the waterline (m), and h is the water depth.

Table 2. Range of velocity during CFD simulation

Velocity (*Vs*) of full-scale (knots)	Velocity (*Vs*) of scale model (m/s)	Froude Number (*Fr*) model scale	Depth Froude Number (F_{rh}) h_w = 0.36 m	Depth Froude Number (F_{rh}) h_w = 2.60 m
12.00	1.455	0.25	0.77	0.29
13.55	1.643	0.28	0.87	0.33
15.06	1.826	0.31	0.97	0.36
16.05	1.946	0.33	1.04	0.39
17.05	2.067	0.35	1.10	0.41

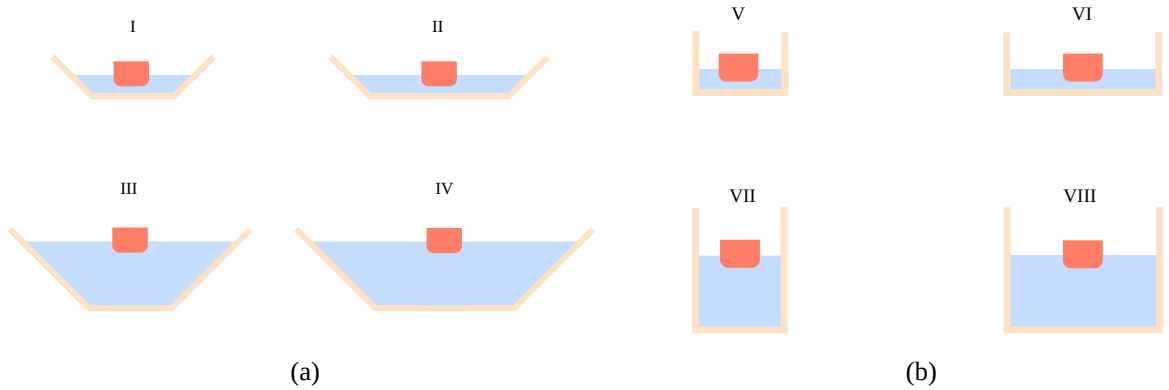

Fig. 3 Illustration of test configuration: (a) Cases I-IV, (b) Cases V-VIII.

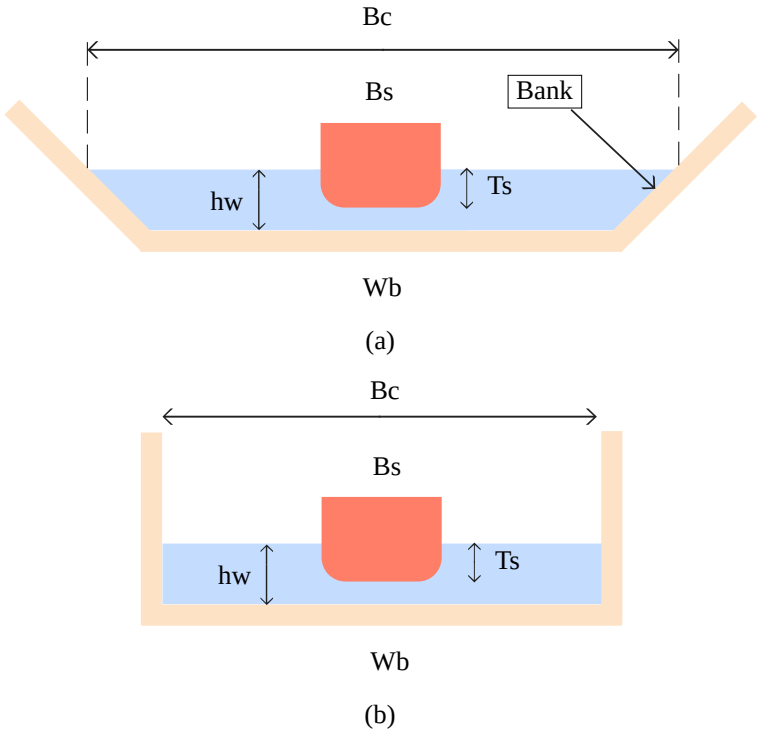

Fig. 4 Canal cross-section of (a) canal bank, (b) rectangular canal.

Table 3. Test configuration and parameters for a canal bank

Cases	W_b (m)	h_w (m)	h_w/T	B_c (m)	B_s (m)	B_c/B_s	m_b
I	2.4	0.36	2.24	3.65	0.644	5.67	0.089
II	4.8			6.05	0.644	9.40	0.050
III	2.4	2.60	16.15	11.41	0.644	17.70	0.005
IV	4.8			13.81	0.644	21.44	0.004

Table 4. Test configuration and parameters for rectangular canal

Cases	W_b (m)	h_w (m)	h_w/T	B_c (m)	B_s (m)	B_c/B_s	m_b
V	2.4	0.36	2.24	2.4	0.644	3.73	0.112
VI	4.8			4.8	0.644	7.45	0.056
VII	2.4	2.60	16.15	2.4	0.644	3.73	0.016
VIII	4.8			4.8	0.644	7.45	0.008

where A_c is canal cross-sectional area (m^2), A_s is the midship area (m^2), B_c is canal surface width, h_w is ship's draft, Fr is Froude Number, W_b is canal bottom width, B_s is ship width, and m_b is blockage ratio (A_s/A_c). Fig. 3a shows the illustration of Cases I-IV, which is a cross-sectional geometry of the canal bank. The illustration of the test configuration in the rectangular sectional geometry of the canal can be seen in Fig. 3b. Fig. 4 compares cross-sectional geometry between canal banks and rectangular canals.

2.3 Computational Domain and Boundary Conditions

The size of the computational domain and the boundary conditions are essential factors that affect CFD simulation results. As depicted in Fig. 5-7, these computational settings have three computational domains: validation test, canal bank, and rectangular canal resistance test. Compared with the results of the total resistance of the IHL towing tank experiment at the same speed, the computational domain used for the validation test aims to verify the developed CFD settings and environment, as seen in Fig. 5. It has been established that CFD simulations should be used to assist towing tank investigations to lessen uncertainty [32].

Fig. 6 and 7 illustrate a computational domain used both for the canal and rectangular banks, with computational parameters corresponding to the validation domain's conditions. The x-axis in the coordinate system was aligned with the ship's length. The y-axis was parallel to the ship's breadth, and the z-axis pointed vertically upwards. The point of origin was at the longitudinal centre of gravity (LCG), and the ship's draft was adjusted to the coordinates based on the ship's hydrostatic data. The dimensions of the upper domain were 1.25 *Lwl* from the free surface, 1.5 *Lwl* from the forward perpendicular (FP), and 2.5 *Lwl* from the after perpendicular (AP) [31]. However, in the validation domain, the bottom was 1 *Lwl* away from the keel. The dimensions of the canal bank domain and the rectangular canal below the water level and centreline were varied to analyze the effect of the width and depth of the canal on the ship's resistance. This study has four types of boundary conditions; velocity inlet, symmetry plane, pressure outlet, and wall [28].

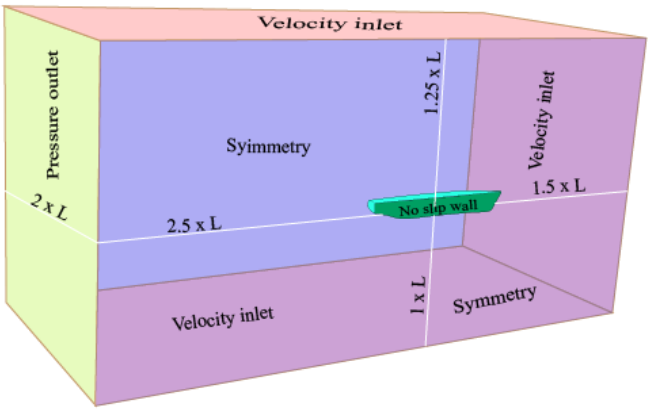

Fig. 5 Computational domain and boundary conditions for a benchmark test.

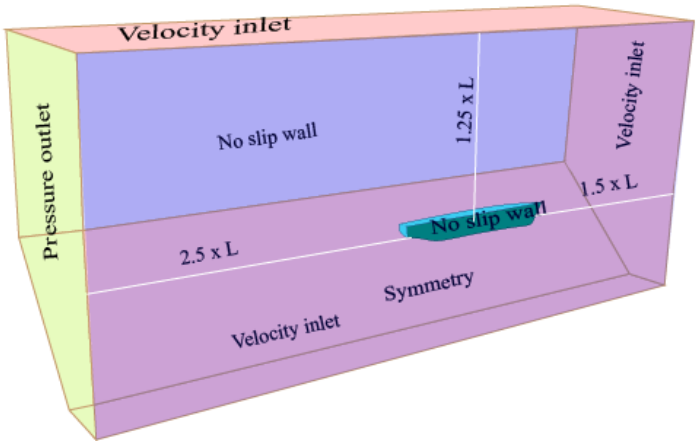

Fig. 6 Computational domain and boundary conditions for canal bank [28].

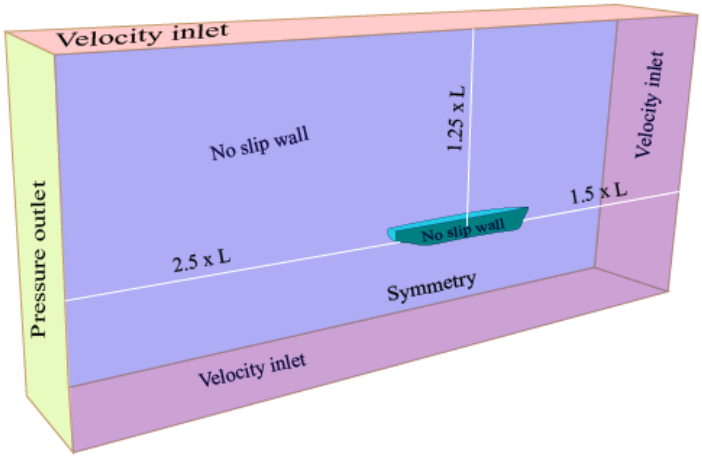

Fig. 7 Computational domain and boundary condition for rectangular canal [28].

2.4 Computational Mesh Strategy

Validation was carried out before simulating the case variations by comparing the results of the total resistance to the IHL experiment. In the current study, the validation case is shown to be the most challenging; in other words, it requires the highest numerical precision so that its validation may be appropriately applied to various simulation settings. The automatic

meshing capabilities in STAR-CCM+ were used to generate meshing. The mesh used in this calculation consisted of hexahedral cells using the overset method (donor-acceptor cell method) [33].

There are two places where free surface enhancements were applied to the background grid: the background as the donor and the overset as the acceptor. A finer grid was created in the area using volumetric controls to capture the flow around the hull near the free surface [34]. The free surface grid must be small enough to capture the wave elevation to enhance the accuracy of the results while also reducing the simulation time. The resulting ship grid was characterized by a concentration of cells on the free surface of the hull grid dependency studies have been made for three grids (Grid 1, Grid 2, Grid 3) with corresponding cell numbers of 3.9, 4.3, and 4.6 million. Table 5 shows the errors in the numerical results for all three grids combined with the experimental resistances. The difference between the experiment data, denoted as *P*, and the CFD simulation results, denoted as *D* in this paper, is determined as:

$$Error = \left|\frac{(P-D)}{P}\right| 100\% \quad (3)$$

Table 5. Mesh dependence study at *Fr* 0.25.

Parameter	EXP (P)	Grid 1 (D)	Grid 2 (D)	Grid 3 (D)
Total Resistance (N)	16.46	15.06	15.53	16.64
Error (%)	-	8.51	5.66	1.09

The presented cases demonstrate that the resistance changes monotonically with mesh density, and the comparison shows a reasonably good agreement between simulation (CFD) and experimental (EXP) values. The minimum error can be founded at *Fr* 0.25, achieved by Grid 3. As a result, Grid 3 is utilized for all case variations, as shown in Table 6.

Table 6. The number of cells, faces, and vertices between different case simulations

Test case	Number of cells	Number of faces	Number of vertices
Validation test	4,551,933	13,651,484	4,801,848
Case I	2,698,239	8,005,214	2,872,508
Case II	3,147,951	9,366,625	3,347,860
Case III	3,581,436	10,688,251	3,797,783
Case IV	4,048,024	12,106,379	4,280,361
Case V	2,492,924	7,389,768	2,651,484
Case VI	2,944,573	8,757,765	3,122,834
Case VII	2,513,540	7,455,738	2,673,789
Case VIII	2,966,083	8,831,445	3,145,905

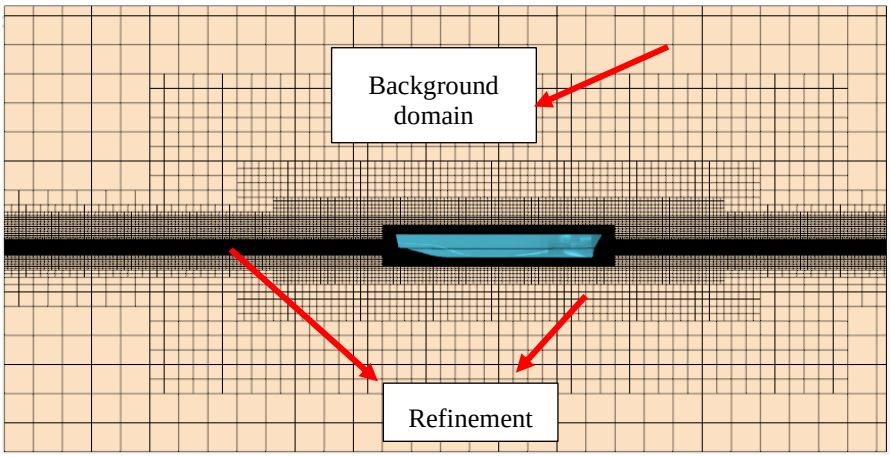

(a)

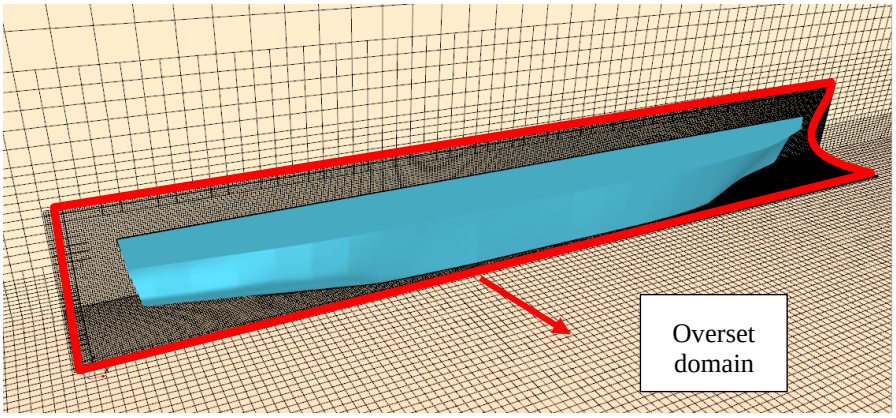

(b)

Fig. 8 Computational mesh overview on: (a) profile view, (b) perspective view

2.5 Numerical Simulation Environment

The CFD simulation was carried out using the RANS solver with the finite volume method. The RANS equation is a time-averaged solution to the Navier-Stokes equation. The flow was assumed to be incompressible due to the water phase [24]. $k-\varepsilon$ model was used in the equation because the RANS equation considers the turbulent impact. Compared to the turbulent SST model, which has a close to 25% increase in CPU time, the $k-\varepsilon$ model is relatively cost-effective in terms of CPU time [27]. $k-\varepsilon$ model is a two equations model that uses turbulent kinetic energy k and turbulent dissipation rate ε . Eq. 4 is used to calculate the $k-\varepsilon$ model [35]:

$$\mu_t = \rho C_\mu \frac{k^2}{\varepsilon} \tag{4}$$

where μ_t is turbulent viscosity and C_μ is a combination of constants and flow parameters. The finite volume approach incorporates two forms of discretization, one in space and one in time. The computing domain was partitioned into a set of non-overlapping cells known as a mesh in the area and into a finite number of time steps. [24]. The VOF method accurately tracks surface motion [36]. The VOF model used the same basic equation assumptions as those used to solve single-phase problems for all fluid phases in the domain because they are assumed to have the same velocity, pressure, and temperature. It means that the equation is solved for an equivalent fluid whose properties represent different phases and volume fractions, respectively [27]. The HRIC discretization scheme was used to increase the sharpness of the interface on

the free surface. The ship was modelled with the even keel condition to simplify the results further. In other words, trim and sinkage were not considered. Fluid properties were determined by considering the ship's data during physical experiments; the determination of fluid properties can be seen in Table 7. It is intended as a parameter adjustment when carrying out physical experiments so that the simulation results can provide near-accurate results.

Table 7. Fluid properties used in water and air environments

Environment	Parameter	Symbol	Unit	Value
Water	Density	ρ	kg/m^3	1025
	Dynamic viscosity	μ	Pa s	8.8871E-4
Air	Density	ρ	kg/m^3	1.18415
	Dynamic viscosity	μ	Pa-s	1.85508E-5

Identifying the time steps (Δt) in the simulation is critical. If the value of Δt is too large, the numerical solution may become unstable or provide unrealistic results [18]. Therefore, the ITTC standards were used to determine the time steps in this investigation using Eq. 5 [37].

$$\Delta t = 0.005 - 0.01\ L/U \tag{5}$$

where L is the length of the waterline (Lwl) and U is the ship's speed, the timestep value is obtained in the range of 0.016-0.023, as shown in Fig. 9.

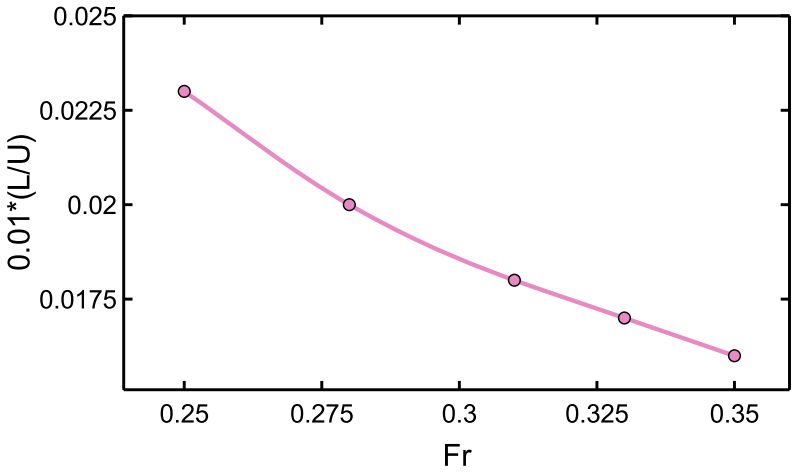

Fig. 9 Timestep simulation at different Froude Numbers.

Prism layers were used to capture the flow behaviour near the wall of the wetted surface. The distance between a cell and the nearest wall is denoted by the $y+$ value, which indicates how well the boundary layer is discretized. The number of prism layers is chosen to ensure an average $y+$ = 30~100 at the ship's wall boundary [10, 31]. Fig. 10 shows the wall y+ contour.

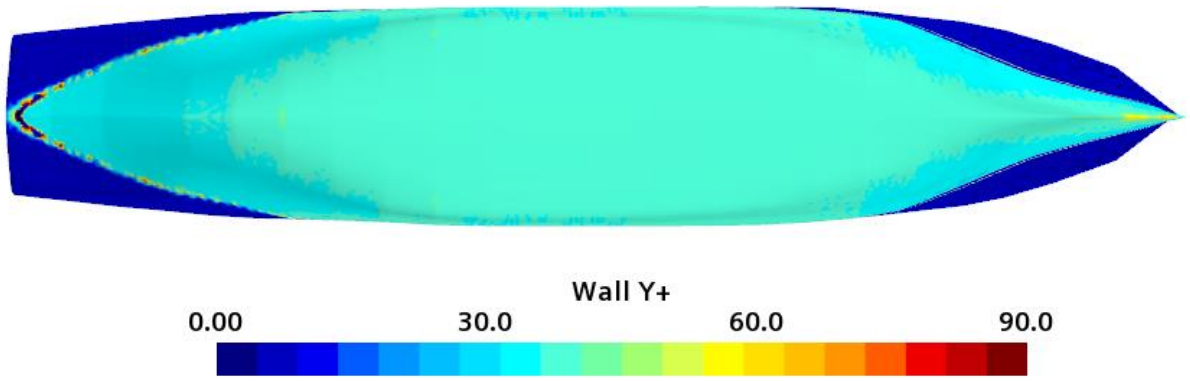

Fig. 10 *y*+ contour on the Perintis 750 DWT ship hull in the range of (0–90)

3. Result and Discussion

3.1 Benchmark study between experimental test and numerical simulation

Numerical validation of total ship resistance was performed using experimental ship resistance data from IHL towing tank in the National Research and Innovation Agency (BRIN) Surabaya, Indonesia. The model test (Model Code LHI 0181) was tested in full load conditions. The computational domain dimensions used to verify the proposed numerical simulation results concerning the ITTC recommendations can be seen in Fig. 5. Fig. 11 shows the testing model and resistance tests at two velocities of 1.455 m/s and 2.067 m/s. The resistance measurements were performed in a large towing tank which was 234.5 m in length (including harbor), 11 m in width, and 5.5 m in depth. A resistance test was conducted by connecting the model to the towing arm, connected to the load cell, and then pulled by the towing carriage at a certain speed. The towing tank was installed in line with the center line of the towing tank and was established in the center of the flotation of the ship model.

According to Table 8, the numerical simulation results were in good agreement with the experimental data, with an error range of 0.11 - 7.74%. Compared with the experimental results, the CFD calculation has a deviation value due to limitations in modelling the environment according to actual conditions. The previous CFD-based studies conducted by Du et al. [9], Elaghbash et al. [38], and Praveen et al. [17] experienced error tolerance in the range of 4-8%. Thus, the deviation value in this study still has a good agreement between numerical and experimental tests. Furthermore, the settings and grid sizes of the benchmark simulation for the IHL experimental test were used to perform simulations on eight case variations.

(a)

(b)

(c)

Fig. 11 (a) model test of the 750 DWT Perintis Ship, (b) resistance at a speed of 1.455 m/s, (c) resistance at a speed of 2.067 m/s.

Table 8. Resistance comparison between IHL experiment and CFD of 750 DWT Perintis Ship

Fr	*Vs* (m/s)	*RT* IHL Exp. (N)	*RT* current CFD (N)	Error (%)
0.25	1.455	11.37	11.38	0.11
0.28	1.643	16.46	16.64	1.09
0.31	1.826	23.26	21.99	5.47
0.33	1.946	28.27	26.20	7.32
0.35	2.067	36.37	33.55	7.74

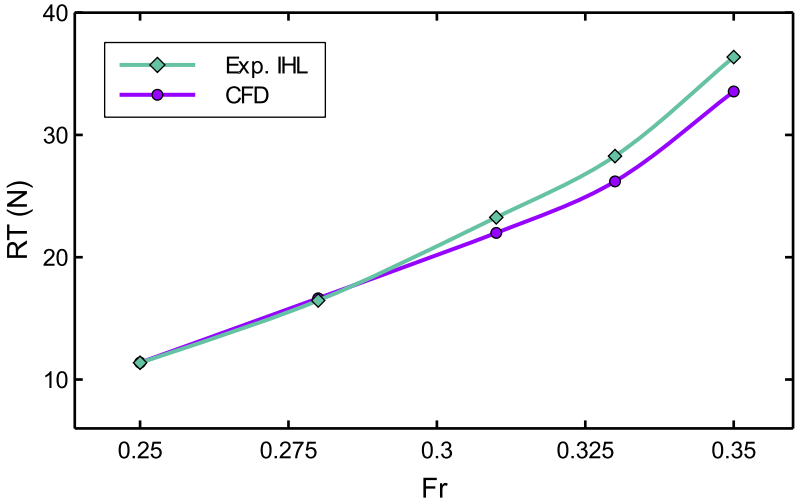

Fig. 12 Resistance value between the IHL experiment and CFD of the 750 DWT Perintis Ship.

3.2 Result of CFD-based resistance simulation

The ship resistance predicted from the RANS produces a force as tangential and normal frictional resistance (R_F) and pressure resistance (R_P) [28]. R_P consists of wave-making resistance (R_W) and viscous resistance (R_V). For total resistance (RT) defined as shown in Eq. 6 [4]:

$$RT = R_F + R_P \tag{6}$$

According to the numerical simulation results, the case with shallower water depth and narrower canal width has a higher resistance value since the ship is in more restricted conditions. In restricted waters, backflow occurs around the ship's hull due to the limited space, affecting the ship's hydrodynamic characteristics and increasing the resistance value. [11].

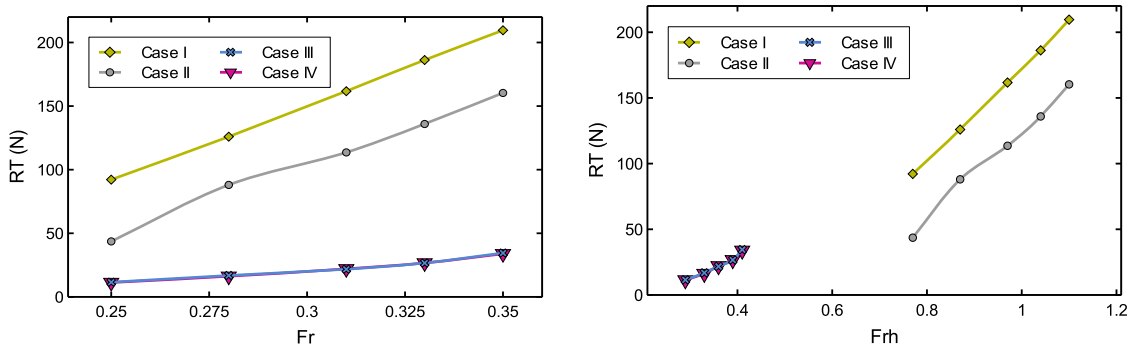

Fig. 13 Resistance value (*RT*) versus Froude Number (*Fr*) and depth Froude Number (*Frh*) in canal bank (Cases I-IV).

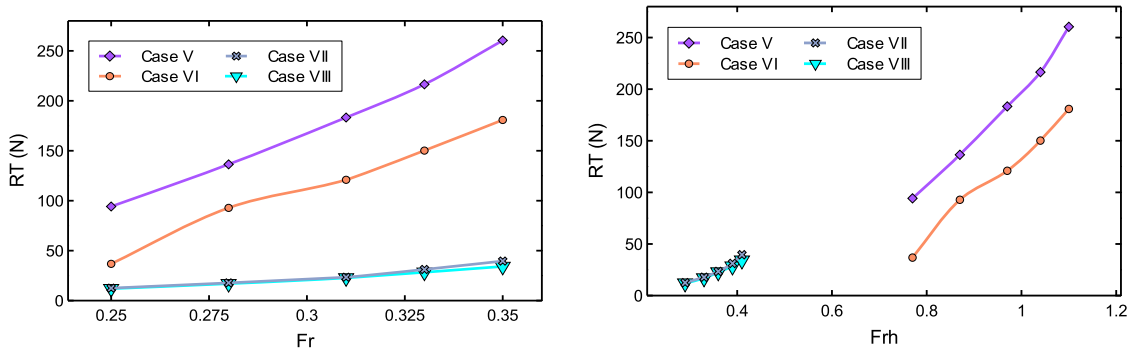

Fig. 14 Resistance value (RT) versus Froude Number (Fr) and depth Froude Number (F_{rh}) in rectangular canal (Cases V-VIII).

Table 9. The total resistance of numerical simulation results in all cases.

Fr	F_{rh} h_w=0.36 m	F_{rh} h_w=2.60 m	Total resistance (RT), N							
			Case I	Case II	Case III	Case IV	Case V	Case VI	Case VII	Case VIII
0.25	0.77	0.29	92.2	43.6	11.5	11.3	94.2	36.8	12.5	12.0
0.28	0.87	0.33	126.0	88.0	16.8	16.2	136.4	92.8	17.8	16.9
0.31	0.97	0.36	161.7	113.6	21.7	22.0	183.3	120.9	23.4	22.7
0.33	1.04	0.39	186.2	135.9	26.6	26.7	216.5	150.2	31.2	28.4
0.35	1.10	0.41	209.6	160.3	34.5	33.9	260.4	180.8	39.6	34.2

The results of the numerical simulation in Cases I-VIII can be seen in Fig. 13-14 and Table 9. From the result, Case I (W_b = 2.4 m) was compared to Case II (W_b = 4.8 m) at the canal bank, which has the same water depth. The resistance value in Case II at Fr 0.25 is 43.61 N, while in Case I, the resistance value was 92.17 N, so there was a significant difference. Likewise, the comparison between Case V (W_b = 2.4 m) and Case VI (W_b = 4.8 m) on rectangular canals. It can occur due to the influence of increasing the dimensions of the canal width [24].

The case simulation with the same W_b but different water depths (h_w/T) showed that the resistance value at h_w/T = 2.24 has a higher value than h_w/T = 16.15 because, at h_w/T = 2.24 condition, there was a change in flow velocity in the bottom area and the pressure drop around the ship was significant, so the total resistance increased. It can be shown in Case I compared to Case III. It can be shown that in Case I, the resistance value increased enormously by about 699.69% compared to the resistance value in Case III. Moreover, Case V also experienced an increased resistance value several times, reaching 654.11% from Case VII. The case simulation with W_b = 4.8 m and the highest water level shows no significant change in the total resistance value. However, these differences can be seen in Fig. 13 between Case III compared to Case IV and in Fig. 14 between Case VII and Case VIII.

3.3 Effect of canal width on resistance value

The influence of canal width and depth on total resistance was investigated by comparing the total resistance values in cases with the same parameter as other cases. Cases with the same

h_w/T value were compared to assess the effect on the canal width parameter. Meanwhile, examples with the same W_b value can be compared to evaluate the influence of changes in canal depth.

The measurement of total resistance when the ship was moving in Case I with Case II and Case V with VI, which has a high water depth of h_w/T = 2.24, was carried out to determine the effect of increasing the width of the canal in shallow water. While the ratio of h_w/T = 16.15 aims to determine the effect of increasing the width of the canal in deep waters. In Case II, IV, VI and VIII, there was an increase in the width of the canal base (W_b) by 50%, so the value of the B_c/B_s ratio was increased. Fig. 15a shows the higher total resistance value found in Case I. The resistance value in Case II at low speed (Fr 0.25) was 43.61 N, while in Case I, the resistance value reached 92.17 N. The increase in the resistance value that occurred in Case I compared to Case II reached an average of 52.91%. In addition, Fig. 15b shows the resistance value of Case III was higher than Case IV. Case IV also experienced an increase in the width of the canal base (W_b) by 50% compared with Case III. The average increase in the resistance value in Case III compared to Case IV was 1.29%, so increasing the width has almost no effect on the total resistance value.

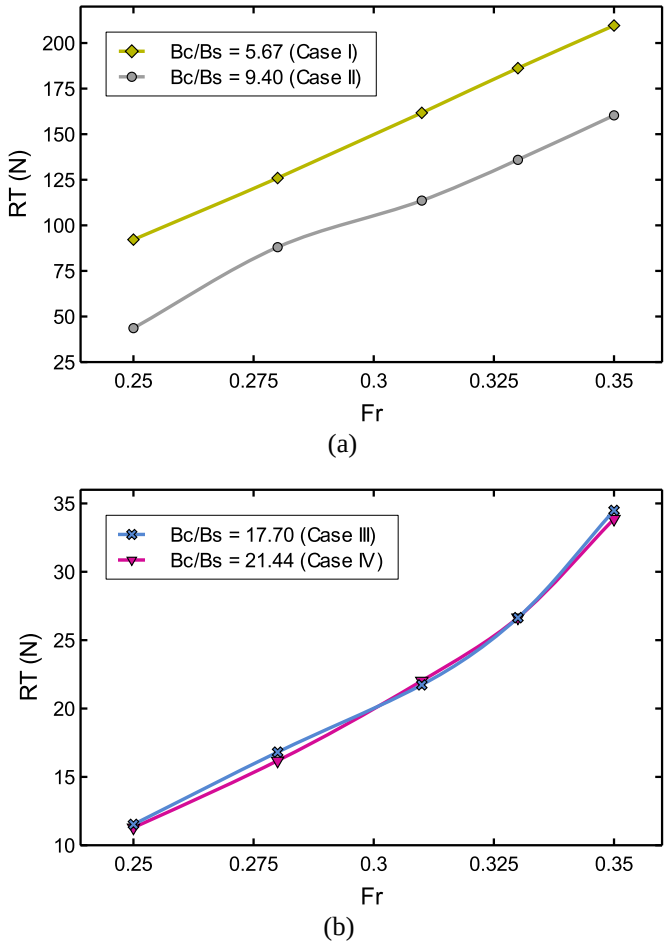

Fig. 15 Resistance value (RT) in canal bank at (a) h_w/T = 2.24, (b) h_w/T = 16.15.

Fig. 16 shows that the total resistance value of Case V was higher than Case VI. In Case VI, the base width of the canal was increased by 50% of the width of the bottom of the canal in Case V. The average increase in the resistance value in Case V compared to Case VI was 68.52%, so it can be analyzed that there was a significant increase in total resistance. At low

speed (*Fr* 0.25), the resistance value in Case V reached 94.22 N, and Case VI was 36.81 N. Moreover, Fig. 16b compares Case VII and Case VIII, which have h_w/T = 16.15 or deep water conditions. However, the bottom canal width in Case VIII was 50% longer than in Case VII. It can be seen that the total resistance value of Case VII was higher than Case VIII. The average increase in Case VII compared to Case VIII was 7.66%. It can be further noted that the addition of the canal bottom width at h_w/T = 16.15 did not increase significantly.

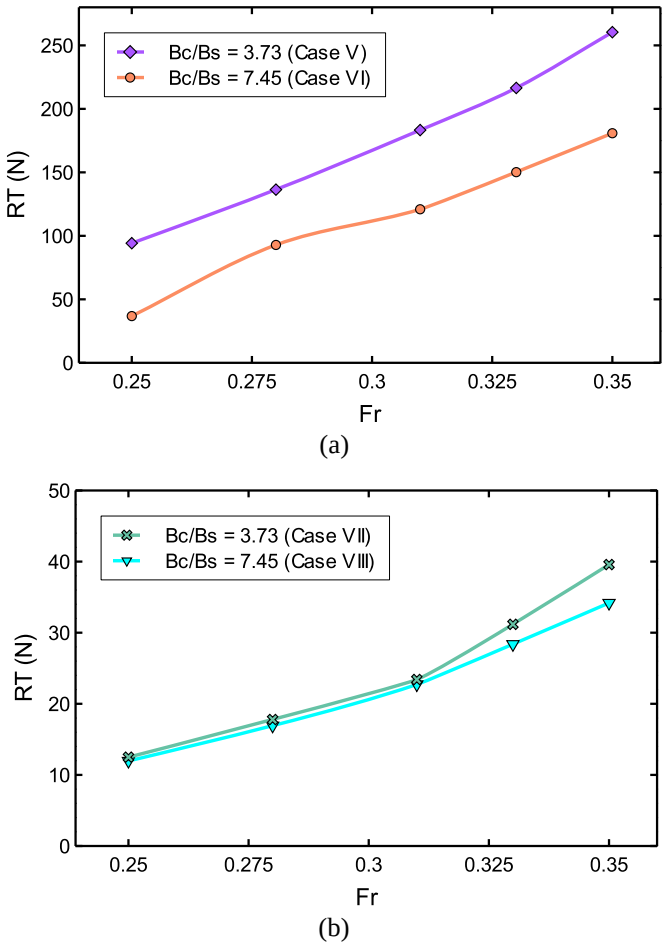

Fig. 16 Resistance value (*RT*) in the rectangular canal at: (a) h_w/T = 2.24, (b) h_w/T = 16.15.

Based on the obtained results of the effect of variations in the width of the canal base on the total resistance value in the canal bank and rectangular canal, it was known that when the width of the canal bottom was increased, the total resistance value decreased. This phenomenon was caused due to the addition of the canal area transversely so that the value of the blockage ratio (m_b) was getting smaller, resulting in a decrease in resistance. The current result was linear with the experimental results by Elsherbiny et al. [26], who reduced the canal width by 37.5% from the initial cross-sectional area. From the data obtained, the total resistance coefficient increased in the canals that experienced a reduction in width dimensions due to the effect of a higher blockage ratio. It indicated an increase in the flow velocity in the canal, which increased the total resistance value [11]. Moreover, Huang et al. [24] investigated total resistance when the ship passes through the ice canal by comparing the simulation in the open water condition

at *Fr* 0.03 and h_w/T = 0.5. Analyzed at B_c/B_s = 1.1-1.3, it showed that the higher the B_c/B_s value, the total resistance was getting closer to the resistance value in open water conditions.

3.4 Effect of depth ratio (h_w/T) on resistance value

Comparing the total resistance value when the ship was moving in cases with the same width of the canal base was intended to determine the effect of canal depth on shallow waters (h_w/T = 2.24) and deep waters (h_w/T = 16.15). Fig. 17 compares the resistance for canal banks, while the comparison of resistance on rectangular canals is presented in Fig. 18. Fig. 17a and 18a have the same basic width of the canal W_b = 2.4 m. In comparison, Fig. 17b and 18b have a width of the canal W_b = 4.8 m. From the analysis, it can be shown that Case I, Case II, Case V and Case VI have a higher resistance value where the case condition has a value of h_w/T = 2.24. So, comparing the canal depth between h_w/T = 2.24 and h_w/T = 16.15 in both bank and rectangular canals was a significant change in resistance value. In addition, the effect of canal depth on h_w/T = 2.24 significantly increases the total resistance value.

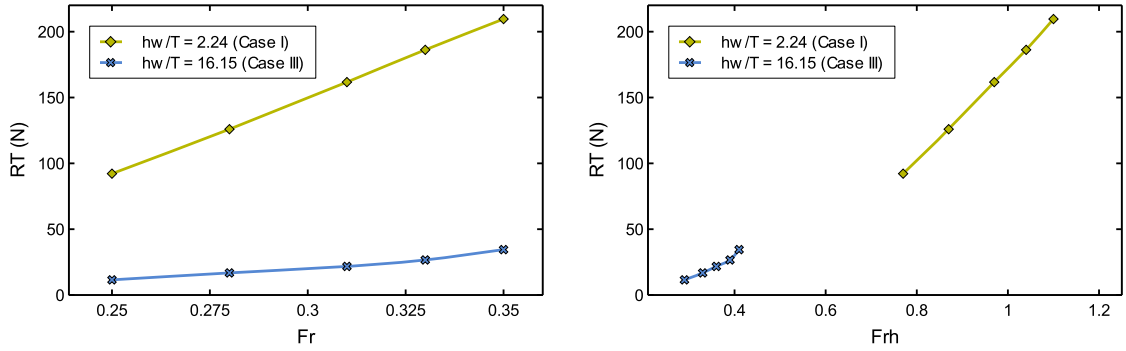

(a)

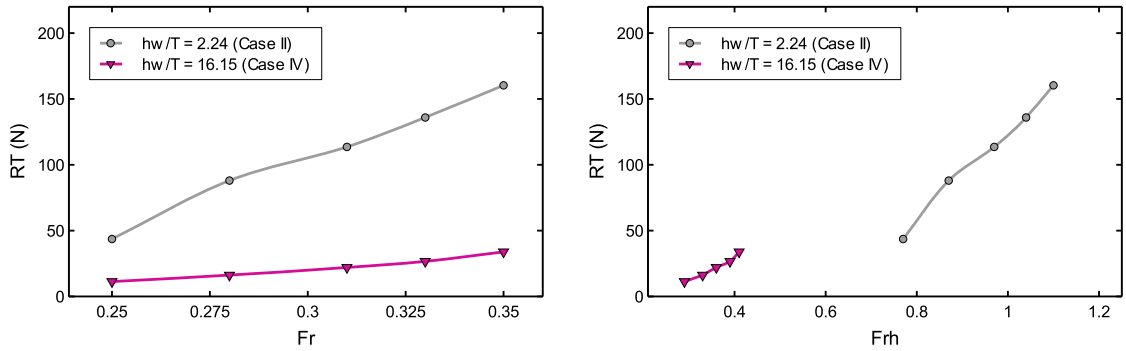

(b)

Fig. 17 Resistance value (*RT*) in canal bank at (a) W_b= 2.4 m, (b) W_b= 4.8 m.

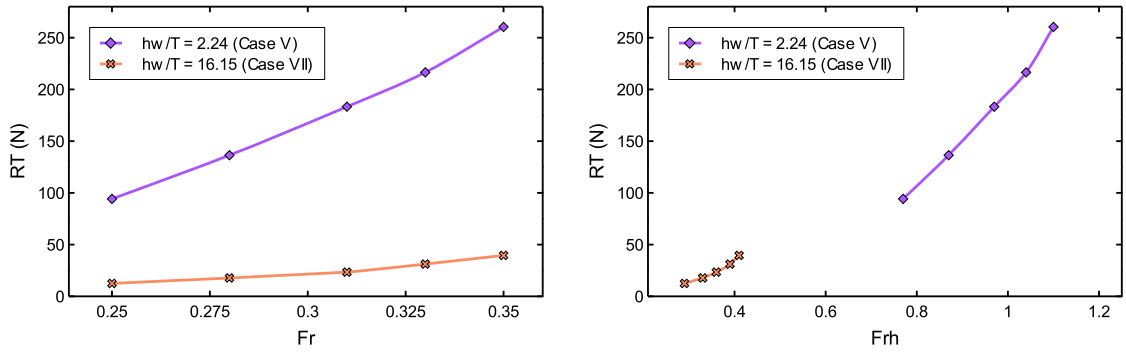

(a)

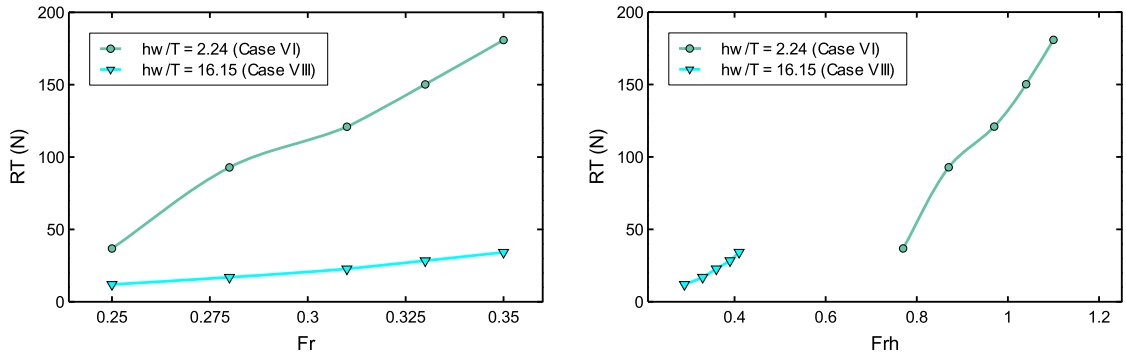

(b)

Fig. 18 Resistance value (*RT*) in the rectangular bank at (a) W_b= 2.4 m, (b) W_b= 4.8 m.

3.5 Effect of blockage ratio (m_b) on resistance value

Due to the effect of canal narrowing, the total resistance coefficient was increased. The greater the blockage ratio, the greater the flow velocity in the canal, which causes the overall resistance value to increase [26]. According to Huang et al. [24], if the ratio of B_c/B_s was larger, the overall resistance value was closer to the resistance value in open water conditions.

The total resistance of the ship in all case simulations was plotted against the blockage ratio (m_b), which can be seen in Fig. 19. The result showed that the higher the blockage ratio, the higher the total resistance value in both canal types. This study expressed the blockage ratio by a non-dimensional equation by comparing A_s/A_c [11, 39]. The curve showed a greater inclination with a higher ship speed. This result proved that ships with higher speeds were more sensitive to changes in waterway restrictions. Ignoring the geometric shape, either canal bank or rectangular canal. Fig. 19 shows that Case IV has the lowest resistance because it was in canal conditions W_b = 4.8 m, B_c/B_s= 21.44, and h_w/T = 16.15. Hence, the cross-section area of the canal becomes wider than in the other cases and causes the blockage ratio value (A_s/A_c) to be small. On the other hand, Case V, where the canal with the narrowest area, resulted in the highest total resistance value compared to other canals.

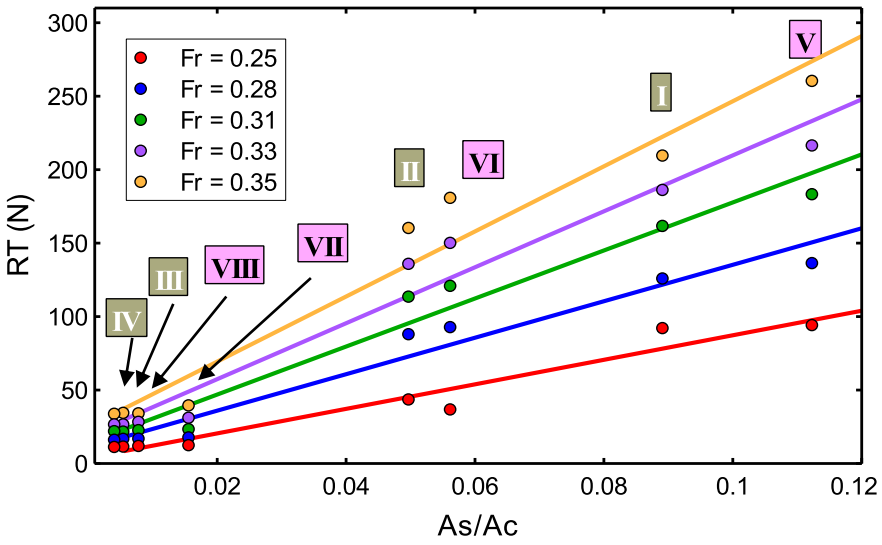

Fig. 19 The total resistance (*RT*) of all simulation cases as blockage ratio function.

The wave pattern generated in the simulation became more complicated as the ship moved through a narrow and shallow canal. Propagation was limited by the edges and bottom of the canal. Reflection and refraction occurred near the wall. The surrounding flow pressure between the hull and the wall was decreased, and the flow can be accelerated in that area. Backflow and subsidence of the free surface became more intensive at a shallow and narrow canal. When the canal width W_b = 2.4 m, the wave pattern generated by the ship rises in the bow and lowers around the hull [11]. As a result, fluid accumulation induced a pressure wave on the bow, causing the pressure force acting on the bow to be greater than the stern [7]. At the same time, the flow velocity decreased in the bow while it increased in the keel [40, 41].

The result followed Bernoulli's principle; an accelerated fluid velocity can result in a pressure drop. The fluid flow in the accelerated keel area caused a pressure drop resulting in a downward force on the hull [42]. This phenomenon was commonly called "ship squat" [11]. In this study, the ship was modelled with an even keel condition, so the ship squat was not considered. The pressure distributions for all cases are shown in Fig. 21. The results demonstrated that the pressure distribution around the ship model was more uniform in the case of hw/T = 16.15. However, in the case hw/T = 2.24, it was seen that a significant high-pressure region was formed at the bow. This observation also explained that pressure increases occurred at low ship-to-bank distances. Relatively heterogeneous pressure contours characterized the pressure variations for narrow and shallow channels. The heterogeneity of the pressure contour was achieved at the bow due to the pressure accumulation of fluid caused by the ship entering a narrow and shallow region. The pressure decreased from the keel to the stern region due to increased fluid velocity under the keel. It caused the increase of ship resistance in shallow and narrow channels compared to wide and deep channels, leading to wave pattern change. Based on these results, the bow was a sensitive area where a significant increase in pressure was identified. Fig. 22 shows that when the ship-bank distance or the water depth reduces, the flow stagnation point on the bow deflected the flow towards the canal wall so that the flow on the ship's side was significantly accelerated. Further, the flow was directed downward, causing the under-keel flow to accelerate.

The flow velocity distribution is shown in Fig. 20. The flow velocity under the keel in Case V was more significant than in Case VIII because fluid accumulation in the bow due to canal narrowing induced the resistance value to increase, accelerating the flow in the keel. Fig. 22.

illustrates the difference in wave height between Case I and Case IV in front of the ship. It was known that the influence of higher restricted waters, such as the width of the small canal and its shallow depth, contributes to the elevation of waves. When navigating a restricted waterway, the wave pattern became more complicated.

The side and bottom of the canal restricted wave propagation, so backflow and free surface subsidence were more intense than in open water conditions, which caused the simulation process longer. Fig. 23 compares the time series between Case I, Case V, and the validation case with *Fr* 0.35. Simulation on the validation case converged faster than Case I and Case V because there were no width and depth restrictions in boundary conditions.

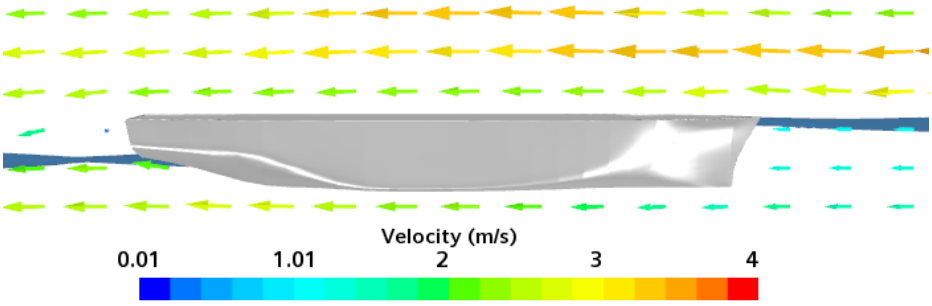

(a)

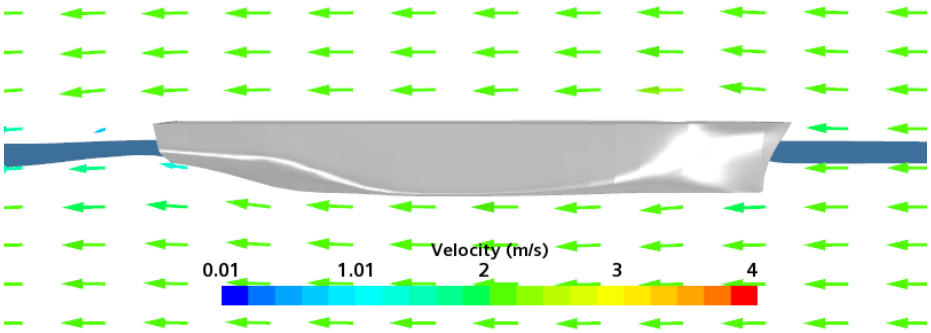

(b)

Fig. 20 Velocity distribution at *Fr*=0.35, the blue surface in each plot represents the free water surface: (a) Case V, (b) Case VIII.

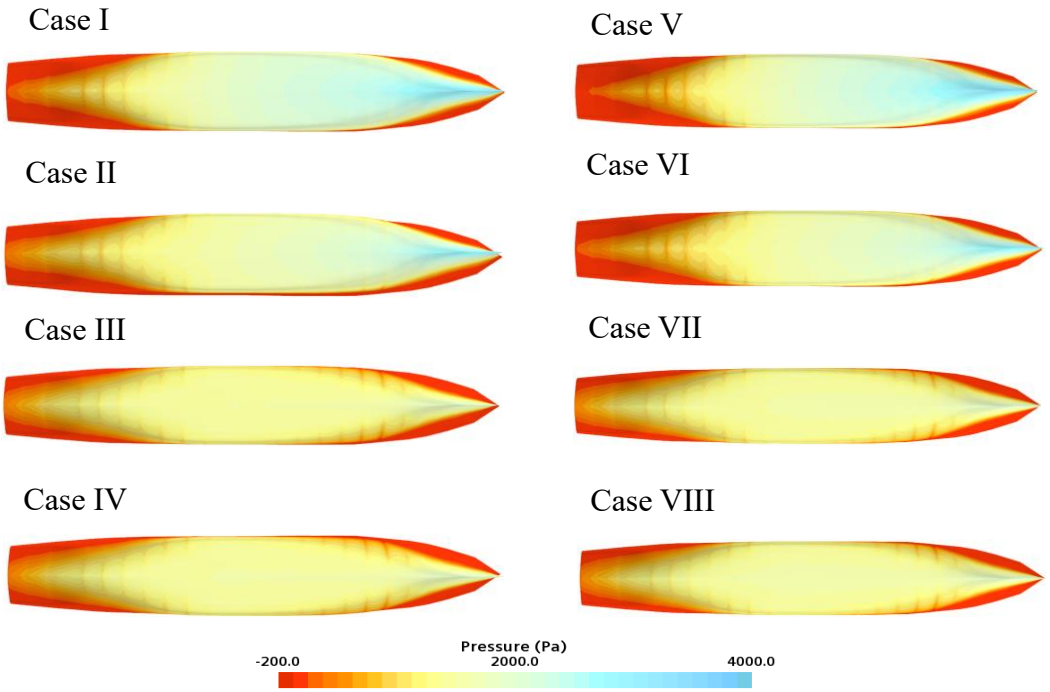

Fig. 21 Pressure distribution in all cases at *Fr* = 0.35.

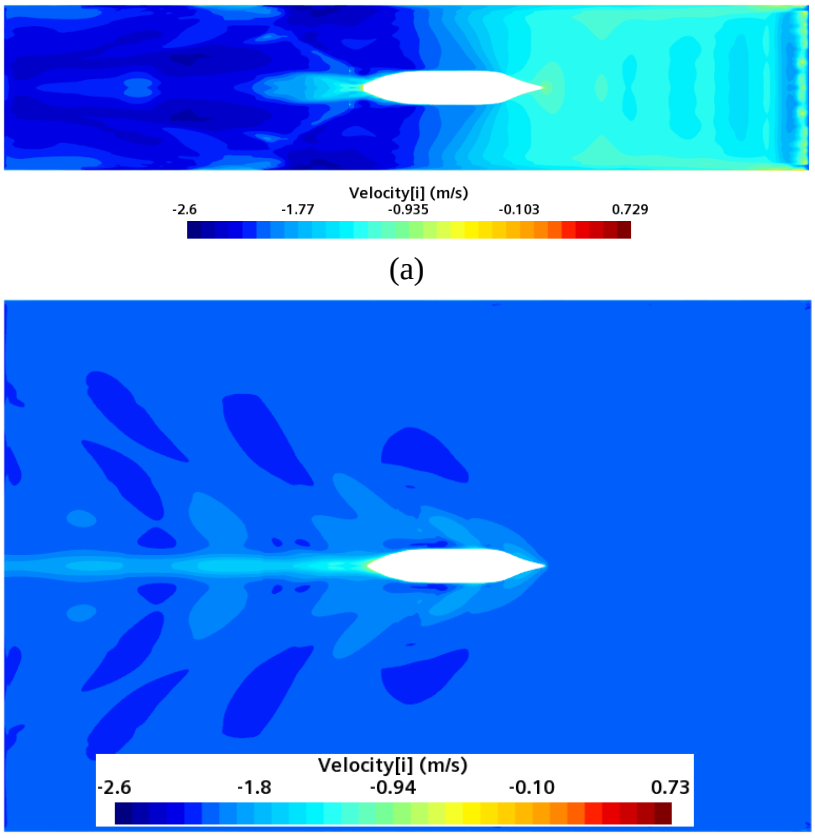

Fig. 22. Water surface *x*-axial velocity distribution at *Fr* = 0.35: a) Case I b) Case IV

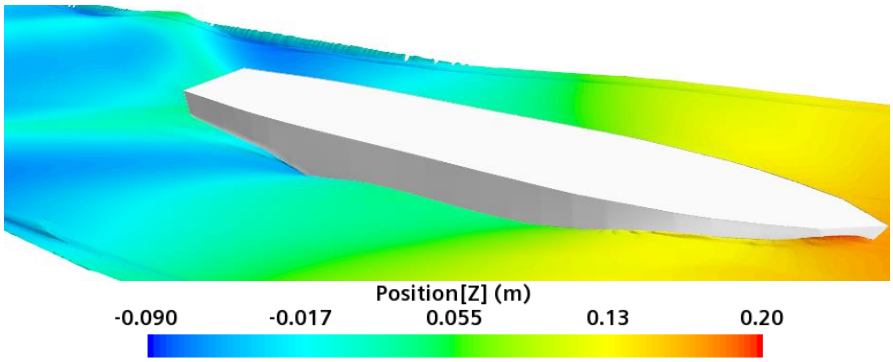

(a)

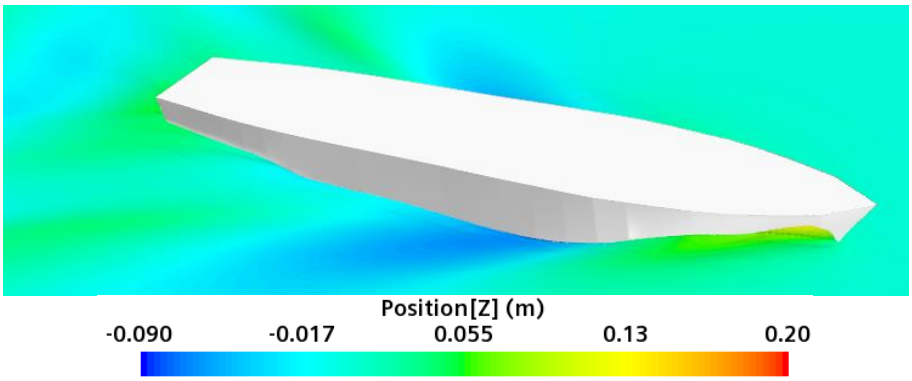

(b)

Fig. 22 Difference of bow wave height at *Fr*=0.35 (a) Case I, (b) Case IV.

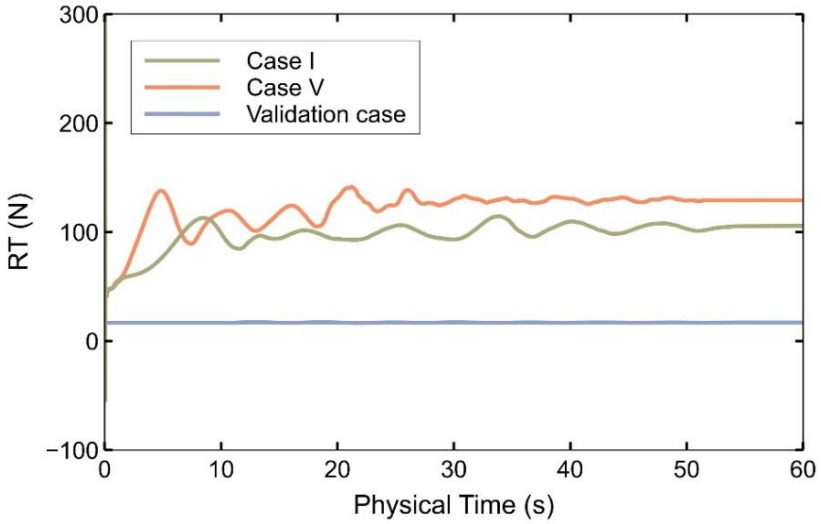

Fig. 23 Comparison of time series between Case 1 and Case IV at *Fr*=0.35.

Fig. 24 illustrates the wave pattern between Case I and Case II at *Fr*=0.35. Both have a comparison value between water depth and ship draft equal to h_w/T = 2.24, but in Case II, it has a value of W_b = 4.8 m. The illustration demonstrated that the divergent wave generated at the stern had no effect on the angle, and there was a superposition with the divergent wave's reflected wave.

Divergent waves generated in the bow section directly collided with the canal wall, and the fluid flow directly opposite the bow became higher, both of which resulted from the

limitation of the canal width. Fig. 25 compares wave patterns at Fr=0.35 for h_w/T = 2.24 and h_w/T = 16.15 with W_b = 4.8 m. The Kelvin wave pattern generated by the bow and stern can be observed. A solid line represented the Kelvin wedge, representing the ship's wave propagation direction.

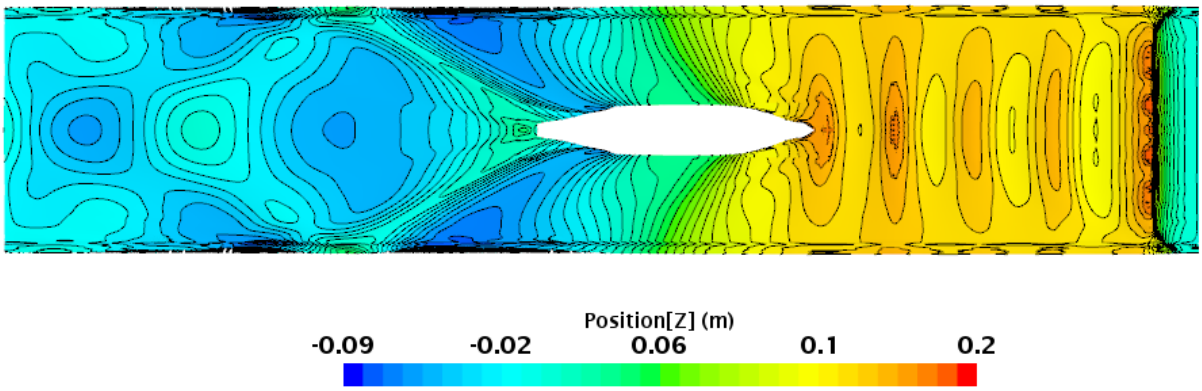

(a)

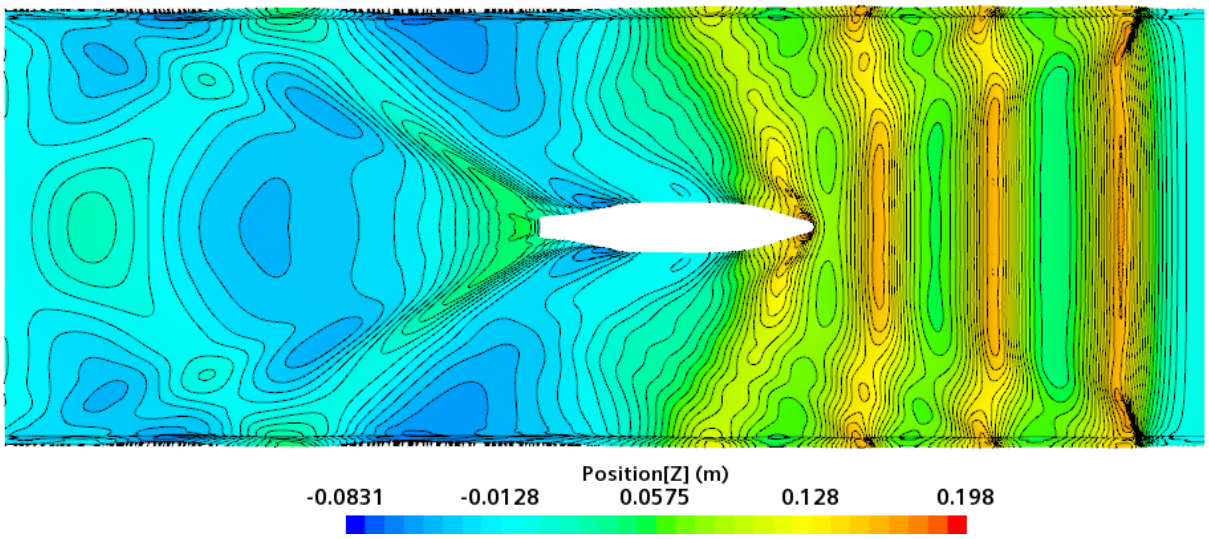

(b)

Fig. 24 Wave pattern at h_w/T = 2.24 and Fr= 0.35 (a) W_b= 2.4 m (Case I), (b) W_b= 4.8 m (Case II).

The Kelvin wave angle in Fig. 25a was greater than in Fig. 25b. It was indicated by the bow section's divergent waves, which appeared shorter due to their initial impact on the bank. The resulting transverse wave at the stern was visible in Fig. 25b. Based on the analysis of Fig. 24 and 25, it was known that the Kelvin wave angle due to changes in the width of the canal did not change obviously, but it changed under different h_w/T conditions [11,28]. Large Kelvin waves at increasing distances from the ship's centreline appeared to break down into smaller components with more considerable wave heights.

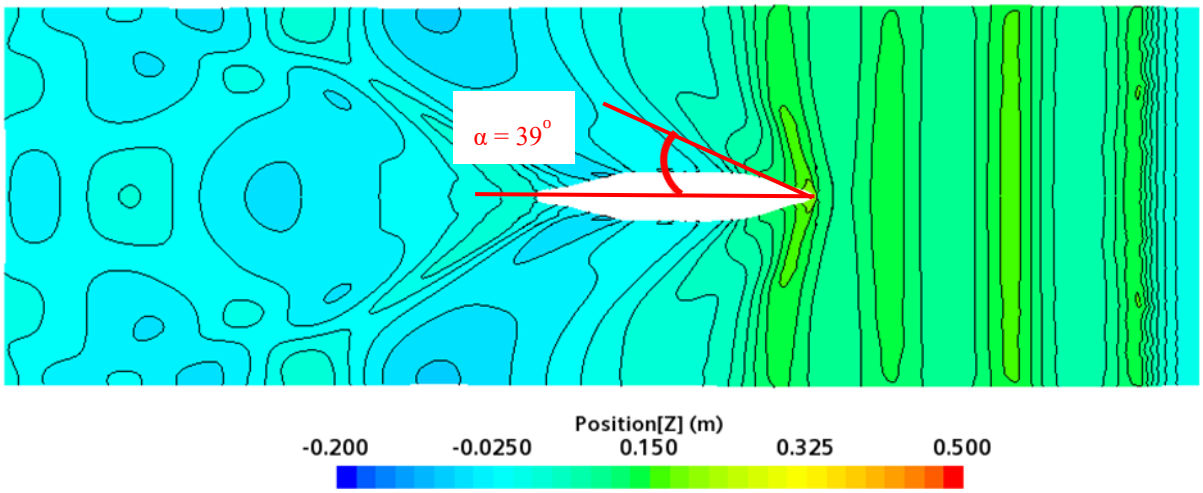

(a)

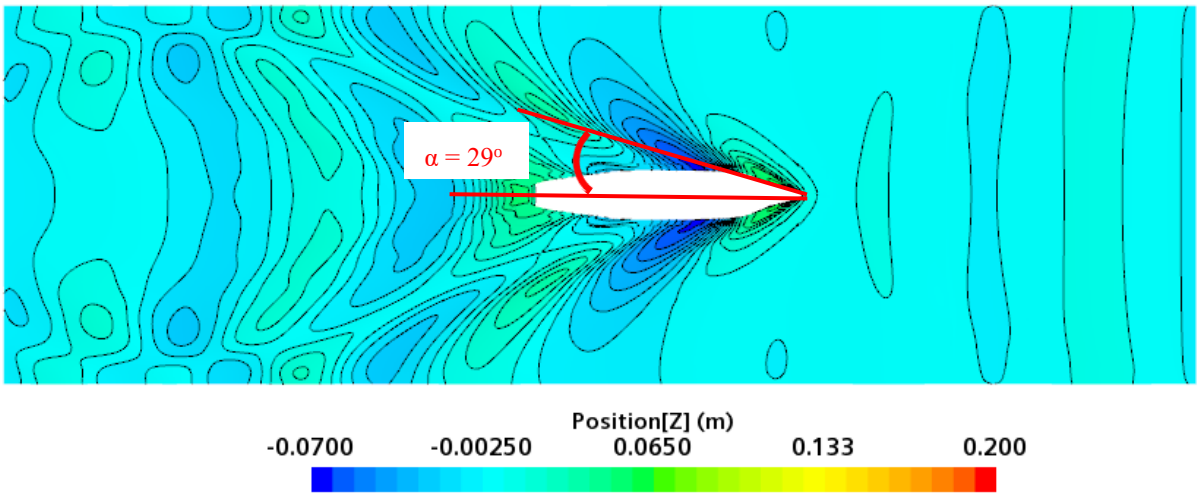

(b)

Fig. 25 Wave pattern at W_b = 4.8 m and Fr = 0.35 (a) h_w/T = 2.24 (Case VI), (b) h_w/T = 16.15 (Case VIII).

4. Concluding Remarks

A series of CFD-based simulations were conducted to investigate the different canal types and cross-sections on resistance and wave-generated characteristics of 750 DWT Perintis Ship. Two different canal types, including canal bank and rectangular canal, were investigated at low and high-speed conditions. In the benchmark study, the proposed CFD simulation results resulted in good agreement with the experimental test, with an error range of 0.11 - 7.74%, indicating the CFD setting and environment can be used in further analysis. The influence of canal types on resistance value results in several phenomena. Similar results were found both in rectangular and canal banks. The case with a shallower (lower h_w/T) and a narrower (lower B_c/B_s) canal dimension has a higher resistance value. The wave pattern generated in the simulation became more complicated as the ship moved through a narrow and shallow canal. Backflow and subsidence of free surface became significant around the ship's hull in more restricted water, changing the ship's hydrodynamic characteristics and increasing resistance. It can be found that the higher the blockage ratio (m_b), the higher the total resistance value in both

canal types, which proved that ships with higher speeds were more sensitive to changes in waterway restrictions.

In addition, changes in the dimensions of the canal width at h_w/T = 16.15 have no significant effect on the total resistance. The results demonstrated that the pressure distribution around the ship model was more uniform at h_w/T = 16.15. In contrast, it can significantly affect h_w/T = 2.24 for both canal bank and rectangular canals. It was seen that a significant high-pressure region was formed at the bow. This observation also explained that pressure increases occurred at low ship-to-bank distances. Relatively heterogeneous pressure contours characterized the pressure variations for narrow and shallow channels. The heterogeneity of the pressure contour was achieved at the bow due to the pressure accumulation of fluid caused by the ship entering a narrow and shallow region.

This finding could become a topic for future research. One possibility is to conduct several CFD-based simulations and towing tank experiments at the basin with similar models and canal cross-sections to investigate the effect of adding a bulbous bow with different geometries on ship resistance increase, wave-generated characteristics, and maneuverability test assessment.

Acknowledgements

The authors are grateful to Research Center for Hydrodynamics Technology, National Research and Innovation Agency (BRIN), Surabaya, Indonesia, which enabled them to carry out the research reported in this current work.

REFERENCES

[1] Hadi, E. S., Manik, P., Iqbal, M. 2018. Influence of hull entrance angle 'Perintis 750 DWT', toward ship resistance: The case study for design development 'Perintis 750 DWT.', *MATEC Web of Conferences*, 159, 2–7, Semarang, Indonesia. https://doi.org/10.1051/matecconf/201815901057

[2] Perhubungan, K. 2016. Peraturan Menteri Perhubungan Republik Indonesia Nomor PM 6 Tahun 2016 Penyelenggaraan Kegiatan Pelayanan Publik Kapal Perintis Milik Negara.

[3] Tual, P. C. 2021. Rute Dan Jadwal KM. Sabuk Nusantara 91, *Pelnitual.co.id*, https://pelnitual.co.id/web/index.php/jadwal-kapal/kapal-sabuk-nusantara/11-load-module/357-rute-dan-jadwal-km-sabuk-nusantara-91.html , accessed 2nd February 2022.

[4] Terziev, M., Tezdogan, T., Oguz, E., Gourlay, T., Demirel, Y. K., Incecik, A. 2018. Numerical investigation of the behaviour and performance of ships advancing through restricted shallow waters, *Journal of Fluids and Structures*, 76, 185–215. https://doi.org/10.1016/j.jfluidstructs.2017.10.003

[5] Lataire, E.,Vantorre, M., Delefortrie, G. 2015. Longitudinally Directed Bank Effects, *Proceeding of the International Conference on Marine Simulation and Ship Maneuverability (MARSIM 2015)*, Newcastle upon Tyne, UK.

[6] Tuck, E. O. 1978. Hydrodynamic Problems of Ships in Restricted Waters., *Annual Review of Fluid Mechanics*, 10, 33–46. https://doi.org/10.1146/annurev.fl.10.010178.000341

[7] Elsherbiny, K., Tezdogan, T., Kotb, M., Incecik, A., Day, S. 2019. An experimental investigation of the trim effect on the behaviour of a containership in shallow water, *Proceedings of the International Conference on Offshore Mechanics and Arctic Engineering - OMAE*, 7B-2019, 1–9, Glasgow, UK. https://doi.org/10.1115/OMAE2019-95790

[8] Rotteveel, E., Hekkenberg, R., van der Ploeg, A. 2017. Inland ship stern optimization in shallow water, *Ocean Engineering*, 141, 555–569. https://doi.org/10.1016/j.oceaneng.2017.06.028

[9] Campbell, R., Terziev, M., Tezdogan, T., Incecik, A. 2022. Computational fluid dynamics predictions of draught and trim variations on ship resistance in confined waters, *Applied Ocean Research*, 126, 103301. https://doi.org/10.1016/j.apor.2022.103301

[10] He, Z., Yuanyuan, H., Cheng, X., Luying, Q. 2021. Model of working ship crossing channel. *Brodogradnja*, 72(1), 125-143. https://doi.org/10.21278/brod71207

[11] Du, P., Ouahsine, A., Sergent, P., Hu, H. 2020. Resistance and wave characterizations of inland vessels in the fully-confined waterway, *Ocean Engineering*, 210, 107580. https://doi.org/10.1016/j.oceaneng.2020.107580

[12] Moustafa, M.M., Yehia, W. 2017. Squat assessment for safe navigation of River Nile cruisers.

Brodogradnja, 68(2), 1-13. https://doi.org/10.21278/brod68201

[13] Zeraatgar, H., Akbari Vakilabadi, K., Yousefnejad, R. 2011. Parametric Analysis of Ship Squat in Shallow Water by Model Test. *Brodogradnja*, 62(1), 37-43.

[14] Ahmed, T. M., Elaghbash, A. O., Banawan, A. A., Ahmed, Y. M., Hassan, A. M. 2020. Numerical Prediction of Solitary Wave Formation of a Planing Hull in Shallow Water Channels. *Brodogradnja*, 71(3), 135-148. https://doi.org/10.21278/brod71308

[15] Ismail, M. A., Shaharuddin, N. M. R., Yaakob, O., Jamal, M. H., Adnan, F. A., Rashidi, A. H. M., Ahmad, N. S. 2022. Wake wash of a fast small boat in restricted waters: model tests and full-scale measurements. B*rodogradnja*, 73(2), 93-119. https://doi.org/10.21278/brod73206

[16] Kim, D., Kim, S. H., Kim, S. J., Paik, K. J. 2017. A study on the sensitivity analysis of the hydrodynamic derivatives on the maneuverability of KVLCC2 in shallow water. *Brodogradnja*, 68(4), 1-22. https://doi.org/10.21278/brod68401

[17] Praveen, D. S. C., Kumar, S., Bhattacharyya, A., Sha, O. P. 2022. Design study of stern tunnel wedge shapes for a low draft shallow water vessel, *Ships and Offshore Structures*, 17(5), 1114-1131. https://doi.org/10.1080/17445302.2021.1894730

[18] Terziev, M., Tezdogan, T., Incecik, A. 2021. Modelling the hydrodynamic effect of abrupt water depth changes on a ship travelling in restricted waters using CFD, *Ships and Offshore Structures*, 16(10), 1087–1103. https://doi.org/10.1080/17445302.2020.1816731

[19] KumarPatel, P., Premchand, M. 2015. Numerical Investigation of the Influence of Water Depth on Ship Resistance, *International Journal of Computer Applications*, 116(17), 10–17. https://doi.org/10.5120/20427-2750

[20] Larsson, L., Raven, H. C. 2010. The Principles of Naval Architecture Series Ship Resistance and Flow. *The Society of Naval Architects and Marine Engineers*, Jersey City, New Jersey.

[21] Hoa, N. T. N., Bich, V. N., Tu, T. N., Chien, N. M., Hien, L. T. 2019. Numerical Investigating the Effect of Water Depth on Ship Resistance Using RANS CFD Method, *Polish Maritime Research*, 26(3), 56–64. https://doi.org/10.2478/pomr-2019-0046

[22] Chen, C., Delefortrie, G., Lataire, E. 2021. Effects of water depth and speed on ship motion control from medium deep to very shallow water, *Ocean Engineering*, 231, 109102. https://doi.org/10.1016/j.oceaneng.2021.109102

[23] Park, J. Y., Nam, B. W., Kim, Y. 2021. Numerical analysis of hydrodynamic loads on passing and moored ships in shallow water, *Processes*, 9(3), 558. https://doi.org/10.3390/pr9030558

[24] Huang, L., Li, M., Romu, T., Dolatshah, A., Thomas, G. 2021. Simulation of a ship operating in an open-water ice canal, *Ships and Offshore Structures*, 16(4), 353–362. https://doi.org/10.1080/17445302.2020.1729595

[25] Mucha, P., Moctar, O. el, Dettmann, T., Tenzer, M. 2018. An experimental study on the effect of confined water on resistance and propulsion of an inland waterway ship, *Ocean Engineering*, 167, 11–22. https://doi.org/10.1016/j.oceaneng.2018.08.009

[26] Elsherbiny, K., Tezdogan, T., Kotb, M., Incecik, A., Day, S. 2019. Experimental analysis of the squat of ships advancing through the New Suez Canal, *Ocean Engineering*, 178, 331–344. https://doi.org/10.1016/j.oceaneng.2019.02.078

[27] Tezdogan, T., Incecik, A., Turan, O. 2016. A numerical investigation of the squat and resistance of ships advancing through a canal using CFD, *Journal of Marine Science and Technology*, 21(1), 86–101. https://doi.org/10.1007/s00773-015-0334-1

[28] Elsherbiny, K., Terziev, M., Tezdogan, T., Incecik, A., Kotb, M. 2020. Numerical and experimental study on hydrodynamic performance of ships advancing through different canals, *Ocean Engineering*, 195, 106696. https://doi.org/10.1016/j.oceaneng.2019.106696

[29] Terziev, M., Tezdogan, T., Demirel, Y. K., De Marco Muscat-Fenech, C., Incecik, A. 2022. Numerical investigation of depth-varying currents on ship hydrodynamics in confined water, *International Journal of Naval Architecture and Ocean Engineering*, 14, 100461. https://doi.org/10.1016/j.ijnaoe.2022.100461

[30] Zentari, L., el Moctar, O., Lassen, J., Hallmann, R., Schellin, T. E. 2022. Experimental and numerical investigation of shallow water effects on resistance and propulsion of coupled pusher-barge convoys, *Applied Ocean Research*, 121, 103048. https://doi.org/10.1016/j.apor.2022.103048

[31] ITTC. 2014. *ITTC – Recommended Procedures and Guidelines - Practical Guidelines for Ship CFD Applications*, *ITTC – Recommended Procedures and Guidelines*

[32] Degiuli, N., Farkas, A., Martić, I., Zeman, I., Ruggiero, V., Vasiljević, V. 2021. Numerical and experimental assessment of the total resistance of a yacht. *Brodogradnja*, 72(3), 61-80. https://doi.org/10.21278/brod72305

[33] Yulianti, S., Samuel, S., Nainggolan, T. S., Iqbal, M. 2022. Meshing generation strategy for prediction of

ship resistance using CFD approach, *IOP Conference Series: Earth and Environmental Science*, 1081(1), 12027. https://doi.org/10.1088/1755-1315/1081/1/012027

[34] Siemens. 2019. Star-CCM+ User Guide

[35] Ferziger, J. H., Perić, M. 2002. Turbulent Flows BT - Computational Methods for Fluid Dynamics, J. H. Ferziger; M. Perić (Eds.), , Springer Berlin Heidelberg, Berlin, Heidelberg, 265–307. https://doi.org/10.1007/978-3-642-56026-2_9

[36] Kan, J., Liu, J., Wang, X., Zhao, B. 2020. Numerical simulations of flow field around a 64 teu inland container ship, *Proceedings of the International Offshore and Polar Engineering Conference*, 2020-(August), 3507–3514

[37] ITTC. 2011. 9.1.0, Practical Guidelines for Ship CFD Applications, *ITTC – Recommended Procedures and Guidelines ITTC*, 1–8.

[38] Elaghbash, A. O. 2021. A CFD Study of the Resistance Behavior of a Planing hull in Restricted Waterways, *Sustainable Marine Structures*, 3(1), 32–55. https://doi.org/10.36956/sms.v3i1.414

[39] Pompée, P. 2015. About modelling inland vessels resistance and propulsion and interaction vessel - waterway Key parameters driving restricted / shallow water effects, (September), 7–11.

[40] Lee, S., Hong, C. 2017. Study on the course stability of very large vessels in shallow water using CFD, *Ocean Engineering*, 145, 395–405. https://doi.org/10.1016/j.oceaneng.2017.09.064

[41] Liu, H., Ma, N., Gu, X. 2021. CFD prediction of ship - bank interaction for KCS under extreme conditions, *Journal of Marine Science and Technology*, 26(4), 1062-1077. https://doi.org/10.1007/s00773-021-00798-x

[42] RoyChoudhury, S., Dash, A. K., Nagarajan, V., Sha, O. P. 2017. CFD simulations of steady drift and yaw motions in deep and shallow water, *Ocean Engineering*, 142, 161–184. https://doi.org/10.1016/j.oceaneng.2017.06.058

Submitted: 25.11.2022.

Accepted: 23.01.2023.

Eko Sasmito Hadi
Department of Naval Architecture, Universitas Diponegoro, Semarang 50275, Indonesia
Tuswan Tuswan
Department of Naval Architecture, Universitas Diponegoro, Semarang 50275, Indonesia
Email: tuswan@lecturer.undip.ac.id
Ghina Azizah
Department of Naval Architecture, Universitas Diponegoro, Semarang 50275, Indonesia
Baharuddin Ali
Research Center for Hydrodynamics Technology, National Research and Innovation Agency (BRIN), Surabaya 60117, Indonesia
Samuel Samuel
Department of Naval Architecture, Universitas Diponegoro, Semarang 50275, Indonesia
Muhammad Luqman Hakim
Department of Naval Architecture, Universitas Diponegoro, Semarang 50275, Indonesia
Muhammad Raaflie Caesar Putra Hadi
Department of Naval Architecture, Universitas Diponegoro, Semarang 50275, Indonesia
Muhammad Iqbal
Department of Naval Architecture, Ocean, and Marine Engineering, University of Strathclyde, Glasgow, UK
Dian Purnama Sari
Research Center for Hydrodynamics Technology, National Research and Innovation Agency (BRIN), Surabaya 60117, Indonesia
Dendy Satrio
Department of Ocean Engineering, Institut Teknologi Sepuluh Nopember, Surabaya 60111, Indonesia